Dynamic spike threshold reveals a mechanism for synaptic coincidence detection in cortical neurons *in vivo*

Rony Azouz and Charles M. Gray*

The Center for Neuroscience, University of California, Davis, CA 95616

Communicated by Donald A. Glaser, University of California, Berkeley, CA, May 3, 2000 (received for review November 2, 1999)

Cortical neurons are sensitive to the timing of their synaptic inputs. They can synchronize their firing on a millisecond time scale and follow rapid stimulus fluctuations with high temporal precision. These findings suggest that cortical neurons have an enhanced sensitivity to synchronous synaptic inputs that lead to rapid rates of depolarization. The voltage-gated currents underlying action potential generation may provide one mechanism to amplify rapid depolarizations. We have tested this hypothesis by analyzing the relations between membrane potential fluctuations and spike threshold in cat visual cortical neurons recorded intracellularly *in vivo*. We find that visual stimuli evoke broad variations in spike threshold that are caused in large part by an inverse relation between spike threshold and the rate of membrane depolarization preceding a spike. We also find that spike threshold is inversely related to the rate of rise of the action potential upstroke, suggesting that increases in spike threshold result from a decrease in the availability of Na^+ channels. By using a simple neuronal model, we show that voltage-gated Na^+ and K^+ conductances endow cortical neurons with an enhanced sensitivity to rapid depolarizations that arise from synchronous excitatory synaptic inputs. Thus, the basic mechanism responsible for action potential generation also enhances the sensitivity of cortical neurons to coincident synaptic inputs.

Cortical neurons process information by transforming a continuously varying spatiotemporal pattern of synaptic input into a train of action potentials. Although the cellular mechanisms underlying this process are not fully understood, one common view treats the cortical neuron as a leaky integration device. In this scheme, irregular synaptic input evokes changes in membrane potential (V_m) that accumulate over a membrane time constant until firing threshold is reached and spikes are generated (1–9). The spike output of such a neuron is proportional to its V_m, and the membrane time constant constrains the cell's sensitivity to the timing of synaptic input. Neurons obeying these simple principles are thought to transmit information in their mean firing rates, and little or no information is thought to be conveyed in the timing of action potentials (refs. 9–10; see also ref. 11).

Although it is generally not disputed that cortical neurons integrate their synaptic input and fire action potentials at rates proportional to V_m, this does not exclude a possible sensitivity to the timing of synaptic inputs (11–15). Evidence from crosscorrelation studies (16–18) and recent demonstrations that cortical neurons can fire spike trains with high temporal fidelity (19–22) support this view. Thus, we can say with some confidence that cortical neurons are sensitive to the timing of their inputs, but how this temporal sensitivity is achieved at the cellular level is not fully understood.

One important component of the temporal sensitivity of cortical neurons may stem from the voltage-gated conductances that underlie the action potential. It is well established that the voltage threshold for spike generation depends on the rate of preceding membrane depolarization (23–27). This effect is determined by the gating kinetics of sodium and potassium channels (28–32), which enhance the sensitivity to rapid depolarizations. Consequently the voltage threshold for spiking should be lower and the cell's sensitivity higher when the membrane potential depolarizes rapidly. Because rapid depolarizations may arise in response to synchronous synaptic input, this suggests that the spike-generating mechanism may amplify coincident inputs. Here, we report that the spike activity of visual cortical neurons recorded intracellularly *in vivo* is consistent with this hypothesis.

Methods

All experiments were conducted on anesthetized (Halothane, 1.0–1.5%) and paralyzed (pancuronium bromide, 0.3 mg/kg/h) adult cats of both genders. The methods for induction and maintenance of anesthesia, surgical preparation, and intracellular recording *in vivo* have been described previously (33–35). Intracellular recordings were obtained by using K^+-acetate-filled (4 M) glass micropipettes beveled to a resistance of 70–120 MΩ. Input resistance and intrinsic firing patterns were assessed by using square wave current pulses (range of −0.5 to + 1.8 nA) (36–37). Cellular receptive fields were mapped by using mouse-controlled light bars and sine wave gratings. Quantitative data were obtained in response to 20–30 presentations of a drifting sine wave grating (10–20 cd/m^2 mean luminance, 80-Hz noninterlaced refresh rate; 1,024 × 768 resolution) presented to the dominant eye at the preferred orientation, direction, velocity, and spatial frequency. The intracellular signals were digitized at a rate of 20 kHz and stored for off-line analysis.

Data Analysis. The aim of our analysis was to measure the *voltage* threshold for each spike in each cell and to determine whether fluctuations in threshold were related to several measures of cellular activity. To eliminate putative intradendritic recordings from our sample, only cells with action potentials that exceeded 0 mV and that did not decrease appreciably in amplitude (>10 mV) during sustained depolarization were included. To measure spike threshold, we identified the voltage preceding each spike, which, once reached, resulted in an action potential (33). We computed the maximum rate of change of V_m $(dV_m/dt)_{max}$ over three consecutive data points (150 μs) during the upstroke of each spike (see Fig. 1*D Inset*) and calculated dV_m/dt for each interval of time preceding the peak slope. Threshold was defined as the voltage at the onset of each spike at which dV_m/dt first reached an empirically determined fraction of $(dV_m/dt)_{max}$. This ratio was chosen when the value of dV_m/dt resulted in a close match to the threshold assigned by careful visual inspection of the raw data. For our data set, this value was 0.033. This number

Abbreviations: HH, Hodgkin–Huxley; CTA, cycle-triggered average; EPSP, excitatory postsynaptic potential; FS, fast spiking.

*To whom reprint requests should be addressed. E-mail: cmgray@ucdavis.edu.

The publication costs of this article were defrayed in part by page charge payment. This article must therefore be hereby marked "*advertisement*" in accordance with 18 U.S.C. §1734 solely to indicate this fact.

Article published online before print: *Proc. Natl. Acad. Sci. USA*, 10.1073/pnas.130200797. Article and publication date are at www.pnas.org/cgi/doi/10.1073/pnas.130200797

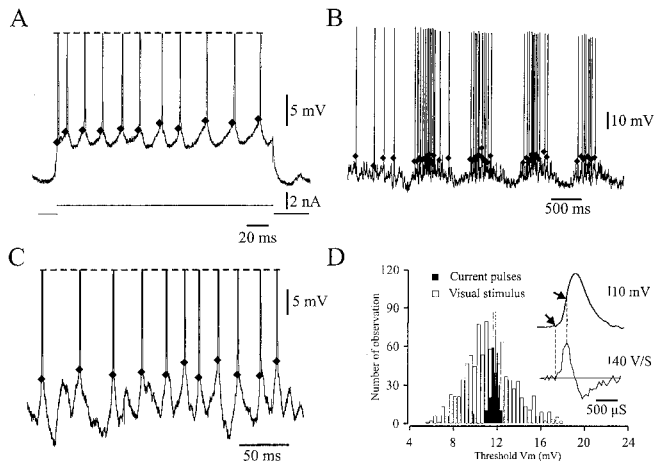

Fig. 1. Action potential threshold shows marked variation in response to visual stimulation but not depolarizing current pulses. The data are taken from a layer II/III regular spiking pyramidal neuron with a simple receptive field. (*A*) Response of the cell to a suprathreshold depolarizing current pulse (900 pA, 200 ms). In this and the other plots, spike threshold is indicated by the filled diamonds. (*B*) Response of the same cell to a drifting square-wave grating (0.6 cycles/degree) presented to the dominant eye. (*C*) An expanded view of the activity in *B* during the peak of one cycle of the visual response. (*D*) Histogram of spike thresholds in response to the depolarizing current pulses (filled bars; $\sigma = 0.34$ mV) and the visual stimulus (unfilled bars; $\sigma = 2.5$ mV). *D Inset* illustrates the method for calculating spike threshold. The upper trace shows a single action potential marked by arrows indicating the threshold voltage (*Lower*) and $(dV_m/dt)_{max}$ (*Upper*). The lower trace shows dV_m/dt for the same action potential. The horizontal line in the lower plot indicates a value of 0 for dV_m/dt.

was carefully chosen so that all the spikes in our sample had ratio values that were equal to or less than this value.

To investigate the relation between spike threshold and V_m, we split the signal into its two components, subthreshold V_m fluctuations and spike activity. The spikes were first truncated at their threshold voltages and their times of occurrence (i.e., leading edge) stored at 1 ms resolution. The truncated record of V_m was resampled at 1 kHz, and any remaining voltage transients were removed by applying a sliding three-point median filter. We then computed the baseline spontaneous V_m by calculating the mean V_m across trials from the first 250 ms of data collected on each trial. The V_m and spike thresholds recorded on each trial were then normalized by subtracting the mean baseline V_m from each data point. All estimates of threshold variation were calculated on a trial-by-trial basis. This procedure was necessary, because the mean membrane potential of cortical neurons varies from trial to trial *in vivo* (33), and action potential threshold covaries with mean membrane potential (data not shown).

We applied two additional measures to determine the relation between V_m and spike activity. First, we calculated the spike-triggered-average of V_m over a $\pm$50-ms time lag for all spikes in a session. This measure revealed the average relationship between spikes and the underlying V_m fluctuations (19, 21, 33). Second, we measured the relationship between spike threshold and the rate of V_m depolarization preceding each spike. For this, spikes were selected if they were separated by at least 20 ms from any preceding spike. This enabled us to exclude the influence of high firing rates on this measure [interspike intervals greater than 6 ms duration had no observable effect on spike threshold (data not shown)]. We computed the threshold voltage and the mean rate of change of V_m for the 10-ms period preceding each spike. These data were evaluated for all spikes occurring on each trial by fitting the data points with a monoexponential function and testing for significance by using analysis of variance ($P < 0.05$).

Computer Simulations. We compared the behavior of a single-compartment model neuron endowed with voltage-gated Na^+ and K^+ conductances to that of an otherwise identical integrate-and-fire model. Our aim was to determine how the rate of V_m depolarization varies with excitatory synaptic input synchronization, and what influence this has on spike threshold. We conducted the numerical simulations by using NEURON (38) and modeled the cell as a single isopotential compartment ($R_m = 125$ KΩ cm^2, $C_m = 1$ μF/cm^2, and $R_{in} = 300$ KΩ; resting $V_m = -70$ mV). Voltage-gated Na^+ and K^+ conductances were implemented by using the Hodgkin–Huxley (HH) equations (28–31). The maximal conductances and the activation and inactivation variables were derived from the data of Huguenard *et al.* (39) and Belluzzi *et al.* (40). The model cell received up to 2,500 excitatory synaptic inputs of the voltage-independent α-amino-3-hydroxy-5-methyl-4-isoxazolepropionic acid (AMPA) type ($V_{rev} = 0$ mV). The time course of the synaptic conductance followed an α function (rise time = 1 ms) and arrival times were Gaussian distributed. Individual synaptic inputs were adjusted so that 200 synchronously occurring excitatory postsynaptic potentials (EPSPs) would evoke a spike in 95% of the simulations of the HH model. The resulting unitary conductance had a peak of 1.5 ns, evoking a peak depolarization of 75 μV at resting V_m. These parameters ensured smooth changes in V_m. Spike threshold of the integrate-and-fire model was set to the minimum threshold of the HH neuron.

To evaluate the effects of input synchrony on the rate of subthreshold V_m depolarization and spike threshold, we varied the standard deviation (σ) of the synaptic arrival times. Input arrival times were randomly chosen so that each presentation of the stimulus yielded a distinct pattern of postsynaptic V_m depolarization. For a given value of σ, we averaged the results obtained from 500 simulations and determined the number of synaptic inputs needed to evoke a spike in 95% of the runs. We then determined the relations between input variance (σ_{input}), rising slope of the subthreshold V_m, spike threshold, and number of synaptic inputs.

Results

Our sample consisted of 47 neurons. In each cell, we compared the distributions of spike threshold in response to depolarizing current steps at two intensities (0.2–0.4 nA and 0.8–1.8 nA) to the distribution measured from the responses to an optimal drifting grating. The standard deviation of each distribution provided a measure of spike threshold variation. An example of the results is shown in Fig. 1. In this cell, 0.9 nA of depolarizing current led to a maintained discharge, a gradual increase in spike threshold, and a slight accommodation in the firing rate (Fig. 1*A*). At this current intensity, the standard deviation of spike threshold was 0.34 mV (Fig. 1*D*, filled bars). In contrast, when the cell was activated by an optimal drifting grating, the spike threshold showed a marked increase in variance (Fig. 1 *B* and *C*). The standard deviation of spike threshold was 2.5 mV (Fig. 1*D*, unfilled bars), representing a 7-fold increase over that seen with depolarizing current pulses. These results were characteristic of our entire sample of cells. Spike threshold variation in response to depolarizing current pulses (low-intensity pulses $\sigma = 0.45 \pm 0.23$ mV; high-intensity pulses $\sigma = 0.83 \pm 0.39$ mV) was on average 3- to 5-fold lower than that found for the visual responses ($\sigma = 2.3 \pm 1.1$ mV).

To determine whether this variability is related to intrinsic cellular properties, we subdivided the cells according to their firing patterns evoked by depolarizing current pulses. As demonstrated previously (34–37), the responses showed four characteristic firing patterns that could be broadly categorized into

Table 1. Spike threshold variability in different intrinsic classes of cortical neurons expressed in millivolts relative to baseline

	RS cells (n = 18)	IB cells (n = 14)	FS cells (n = 5)	CH cells (n = 10)	All cells (n = 47)
Spontaneous activity	1	2	3	4	5
	14.2*[2–4,6] ± 1.2*[6]	16.4*[1,3–4,7] ± 1.4*[7]	4.4*[1–2,4] ± 0.8*[8,1,2,4]	21.1*[3] ± 1.5*[9]	13.8*[10] ± 1.4*[10]
Visual responses	6	7	8	9	10
	16.2*[7–8] ± 2.2*[1]	18.1*[6,8,2] ± 2.6*[2]	5.6*[6–7,9] ± 1.1*[3,6,7,9]	21.2*[6,8] ± 2.5*[4]	15.4*[5] ± 2.3*[5]

RS, regular spiking; IB, intrinsic bursting; FS, fast spiking; CH, chattering. All data expressed as mean ± SD.
*Significantly different ($P < 0.05$) than the indicated subgroup.

regular spiking (RS), intrinsic bursting (IB), fast spiking (FS), and chattering neurons (CH). We compared spike thresholds across these four intrinsic classes. These calculations (Table 1) revealed that the mean and variance of the threshold of FS cells were significantly lower, suggesting that this class of inhibitory interneurons operate closer to threshold and exhibit less threshold variability than other cell classes. With the exception of these cells, we found no significant differences in visually evoked threshold variation among cell classes. The results also revealed that spike threshold variation was lower during spontaneous than during visually evoked activity.

The broad increase in spike threshold variation during visual stimulation suggests that threshold is influenced by the rapid fluctuations in V_m that are prevalent during evoked activity (33). To test this hypothesis, we determined the relation between spike threshold and the rate of change of V_m (dV_m/dt) over a 10-ms period preceding each spike. Because slow fluctuations in V_m may alter spike threshold (data not shown) and its relationship to dV_m/dt, it was necessary to analyze each trial separately. An example of the results is shown for an intrinsic bursting cell in Fig. 2. The plot in Fig. 2*A* shows a short epoch of raw data collected during the cell's response to a visual stimulus. The cell exhibits a relatively broad range of spike thresholds, and many of the spikes appear to arise from rapid V_m depolarizations. This impression is confirmed by the spike-triggered average of V_m shown in Fig. 2*B*, revealing that action potentials tend to be preceded by rapid depolarization. The relation between spike threshold and dV_m/dt preceding each spike is illustrated by the scatter plot in Fig. 2*C*. Spike threshold varied inversely with the preceding dV_m/dt, and this relation was significantly fit by a monoexponential function ($r = -0.75$). We applied the same analysis to 42 of the cells and found a significant correlation on 92% of the trials (639/695 trials; $r_{mean} = 0.61 \pm 0.11$) [FS cells were excluded, because their spike thresholds varied over a much smaller range (Table 1)]. The distribution of decay constants derived from the significant fits is shown in Fig. 2*D* ($\tau_{mean} = 0.94 \pm 0.4$ ms). Together, these data indicate that rapid rates of depolarization lead to lower spike thresholds and suggest that cortical neurons have a greater sensitivity to transient depolarizations arising from synchronous synaptic inputs.

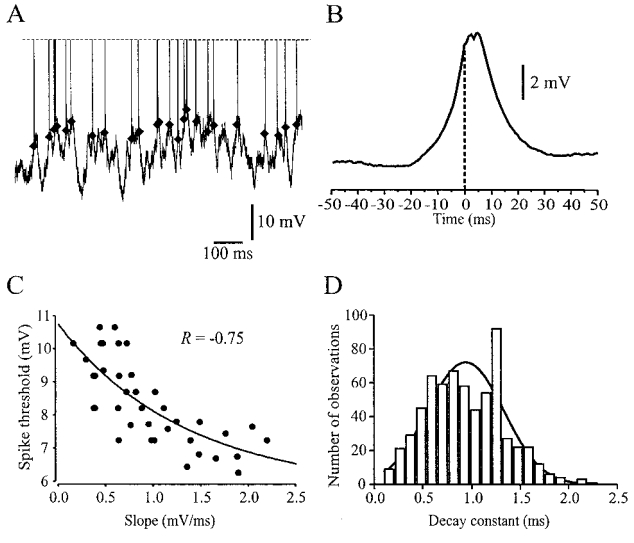

Fig. 2. Spike threshold is inversely correlated with the rate of membrane depolarization. (*A*) Example of the raw data collected from an intrinsic bursting cell during the response to a drifting grating (0.6 cycles/degree) presented to the dominant eye. (*B*) Spike-triggered average of the V_m for all spikes occurring during the presentation of the visual stimulus. The dashed line (time 0) corresponds to the time of action potential generation. The mean rise time (from baseline to peak) for this cell was 12 ms. (*C*) Scatter plot of dV_m/dt preceding a spike vs. spike threshold. The data in *C* were fit by the equation $y = a + be^{-\tau/c}$, where $\tau = dV_m/dt$. (*D*) Histogram of the decay constants (τ) obtained from all trials (639/695) that were significantly fit by the equation in *C*. The mean value is 0.94 ± 0.4 ms.

Because neurons exhibit refractory periods that limit their firing rates, spike threshold will also vary as a function of instantaneous firing rate. To exclude the influence of rapid firing rates, our analysis selected only those spikes that were separated by at least 20 ms from any preceding spike. This raised the question of how much of the variability in spike threshold the V_m time course is responsible for. To address this issue, we calculated the percentage of "single" spikes in the total data set (n = 42 cells) and the range of thresholds covered by correlation with dV_m/dt. We found that the selected spikes constituted 83% of the total spike count, and that the average standard deviation of these spike thresholds was 1.9 ± 0.9 mV. Thus, a substantial fraction (1.9/2.3 = 82.6%) of the total range of threshold variation can be accounted for by the dependence of spike threshold on dV_m/dt.

Because the stimuli used in these experiments led to vigorous suprathreshold responses, the rapid depolarizing transients preceding the spikes might have been due to the activation of voltage-gated conductances and not the result of synchronous synaptic inputs. To estimate the influence of these intrinsic mechanisms, we compared the V_m fluctuations in a subset of the cells (n = 16) under control conditions to those occurring when the cells were hyperpolarized to prevent them from spiking. We applied an analysis to detect the local maxima in the V_m and then calculated the cycle-triggered average (CTA) of the V_m associated with these values. Spikes were removed before this analysis by using the median filter technique. Local depolarizing maxima in the V_m were identified when the central point in a 21-point sliding window (1 ms resolution) was the largest value in the sample. To reduce the influence of noise and eliminate false positives, these local maxima had to be separated from one another by at least 10 ms.

An example of these measurements is shown in Fig. 3. The lower trace in Fig. 3*A* shows the V_m of the cell during the response to the stimulus. The cell showed large transient fluctuations of V_m that often led to spike discharges. The lower trace in Fig. 3*B* illustrates the response of the cell to the same visual stimulus while it was hyperpolarized by a holding current of

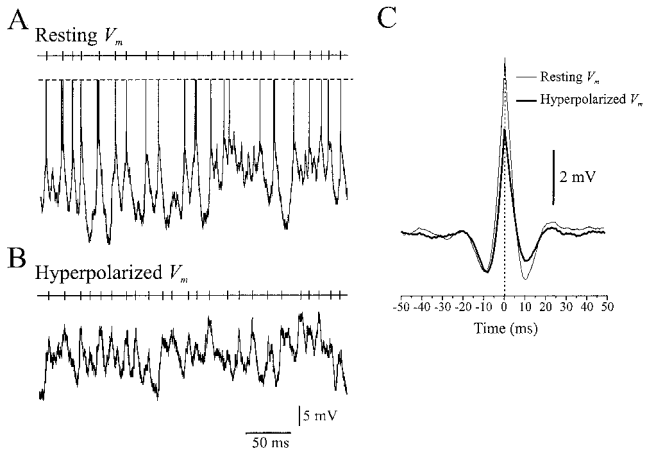

Fig. 3. Membrane hyperpolarization decreases the amplitude and rate of rise of transient depolarizing potentials evoked by visual stimulation. (*A*) The V_m of a layer II/III regular spiking pyramidal neuron (simple cell) recorded during a single presentation of a drifting grating. The action potentials have been truncated as indicated by the dashed lines. (*B*) The response of the same cell to a single presentation of the stimulus, while it was hyperpolarized with a steady negative current to block spike discharges (−2.0 nA). The upper trace in both *A* and *B* indicates the time of occurrence of each local maximum in the median-filtered V_m used to compute the cycle-triggered-average. (*C*) Cycle-triggered averaging reveals that the transient depolarizations evoked by visual stimulation were greater in amplitude and rate of rise during control conditions (6.7 mV, 1.34 mV/ms) than during hyperpolarization (4.5 mV, 1.12 mV/ms).

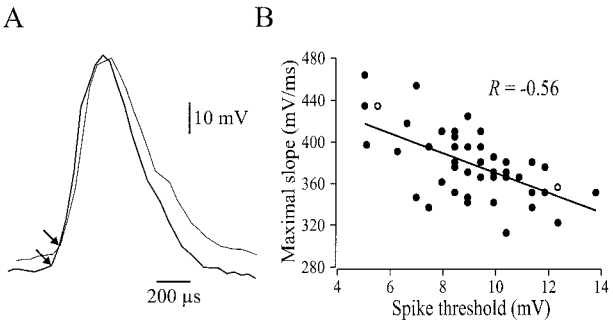

Fig. 4. Spike threshold is inversely correlated with the maximal rate of depolarization during the action potential upstroke. (*A*) Raw data depicting single spikes arising from a different threshold V_m (arrows). Note the difference of the rising slope in the two cells. (*B*) Scatter plot of the visually evoked spike threshold vs. the maximal rising slope taken from one trial. The straight line shows the linear regression fit to the data. The unfilled circles represent the data for the two spikes shown in *A*.

−2 nA. The transient depolarizing fluctuations are still present but somewhat reduced in amplitude. The local maxima detected in these records are shown as vertical tick marks above each voltage trace. These events were used as time stamps to compile the CTAs (computed across trials, ±50 ms time lag) for each cell. Fig. 3*C* shows the CTAs for the same cell during both control (thin line) and hyperpolarized (thick line) conditions. The transient depolarizations were greater in amplitude and rate of rise during control than during membrane hyperpolarization, and a similar relationship was apparent in the remaining cells. In 14 of 16 cells, the peak amplitude of the CTA was greater during control as compared with hyperpolarized conditions ($\text{mean}_{\text{control}} = 4.5 \pm 1.2$ mV; $\text{mean}_{\text{hyper}} = 3.2 \pm 1.0$ mV, $P < <0.001$ paired *t* test). Similarly, in 11 of 16 cells, the rate of rise of the CTA was greater during control as compared with hyperpolarized conditions ($\text{mean}_{\text{control}} = 0.98 \pm 0.42$ mV/ms; $\text{mean}_{\text{hyper}} = 0.77 \pm 0.33$ mV/ms, $P < 0.01$ paired *t* test). These findings indicate that, whereas the rapid changes in V_m are likely to result from synchronous synaptic inputs, their magnitude and rate of depolarization are reduced when the cells are hyperpolarized.

The dependence of spike threshold on dV_m/dt can be partially accounted for by a decrease in the availability of sodium channels due to inactivation. To test this conjecture, we calculated the linear correlation between the firing threshold and the rising slope of the action potential on a trial-by-trial basis. Because the rate of the action potential upstroke provides a sensitive measure of the sodium current, a decrease in the rate of rise would indicate an increase in sodium channel inactivation (43). As before, we excluded FS cells from this analysis because they showed significantly less variation in spike threshold than the other cell classes (Table 1). An example of the results is shown for a chattering cell in Fig. 4. The two traces in Fig. 4*A* show single spikes arising from different thresholds, whereas the plot in Fig. 4*B* illustrates the relation between spike threshold and the rising slope of the action potential in response to a single presentation of the stimulus. The spike threshold was inversely correlated with the maximal rising slope. For the entire sample of cells, we found a similar relation in 83% of the trials (636/766 trials; $r_{\text{mean}} = -0.52 \pm 0.1$). This finding is consistent with the hypothesis that spike threshold increases as a function of sodium channel inactivation (26–30). Thus, the voltage- and time-dependent properties of voltage-gated sodium channels are likely to enhance the sensitivity of cortical neurons to transient membrane depolarization.

We further tested this hypothesis by comparing the behavior of a simple model neuron containing voltage-gated Na^+ and K^+ conductances (i.e., HH neuron) (28–32) to an identical integrate-and-fire model neuron. The modeled cells were activated by a population of excitatory synaptic inputs having Gaussian distributed arrival times. We studied the effects of input synchrony on the rate of V_m depolarization and spike threshold (HH model only) by varying the standard deviation (σ_{input}) of the synaptic arrival times. Example results from two simulations of the HH model are shown in Fig. 5*A*, lower panels. The left panel illustrates the distribution of synaptic arrival times for the two simulations, whereas the right panel shows the responses of the cell to the stimuli. The rate of depolarization was greater, and the spike threshold was lower in response to the more tightly synchronized inputs. This was a general feature of the model over a broad range of input arrival times (Fig. 5*B*). The rate of depolarization increased nonlinearly as a function of input synchronization, and this relation was steeper for the HH panel neuron, indicating that the Na^+ and K^+ currents accelerated the rising slope of the compound EPSP. Similarly, when the magnitude of the compound EPSP was sufficiently large, spike threshold decreased nonlinearly as a function of V_m depolarization rate (Fig. 5*C*), suggesting that fewer synaptic inputs are needed to evoke a spike when those inputs are synchronous. We tested this conjecture by determining the minimal number of synaptic inputs needed to evoke a spike in 95% of the simulations as a function of σ_{input}. This relation increased more rapidly in the HH neuron (Fig. 5*D*), indicating that voltage-gated Na^+ and K^+ channels increase the sensitivity of neurons by lowering spike threshold to coincident synaptic inputs while also decreasing the cell's sensitivity to temporally dispersed synaptic inputs.

Discussion

Our results demonstrate that cortical neurons *in vivo* do not act solely by integrating their synaptic input and firing action potentials when a fixed threshold is reached. Rather spike threshold varies over a broad range of V_m and is sensitive to both the magnitude and the rate of V_m depolarization. Spike thresh-

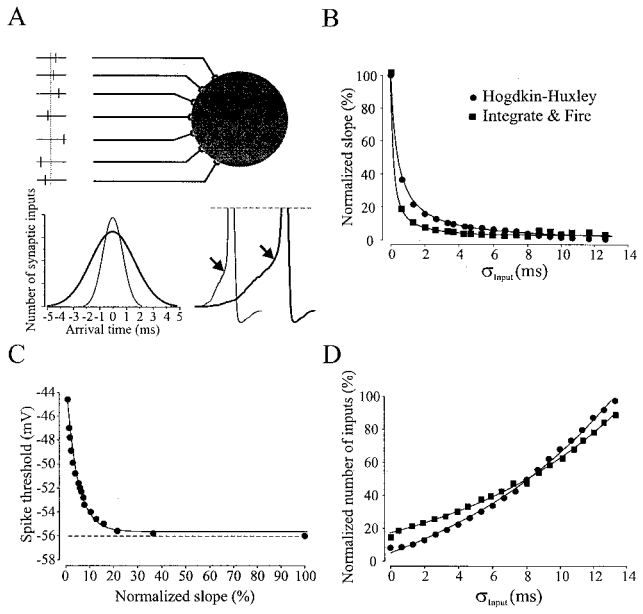

Fig. 5. Spike threshold is inversely correlated with synaptic input synchronization in a model neuron. (*A*) Schematic diagram of the simulation protocol. *Upper* depicts the model neuron (*Right*) and its excitatory synaptic inputs (*Left*). *Lower* shows two examples of the distribution of synaptic arrival times (*Left*) and the corresponding action potentials in the model neuron. Spike threshold is marked by the arrows. (*B*) Plot of σ_{input} vs. normalized V_m slope preceding a spike for HH (filled circles) and integrate-and-fire (filled squares) neurons. The data were fit by the equation $y = 1/(a + bt)$, where $t = \sigma_{input}$. (*C*) Plot of the normalized V_m slope (dV_m/dt) preceding a spike vs. spike threshold. The data were fit by the equation $y = a + be^{-\tau/c}$, where $\tau = dV_m/dt$. The dashed line indicates the firing threshold of the integrate-and-fire neuron. (*D*) Plot of σ_{input} vs. the normalized number of inputs needed to elicit a spike on 95% of the simulated trials for both types of cells. The data were fit by the equation $y = a + be^{c\tau}$, where $\tau = \sigma_{input}$.

olds are lowest when V_m is depolarizing rapidly and highest when the cells are strongly depolarized and firing at high rates. This indicates that the spike-generating mechanism dynamically regulates neuronal output as a function of the magnitude and time course of V_m depolarization (42). We interpret the occurrence of rapid V_m depolarizations as evidence of synchronous excitatory synaptic input, which could also be influenced by the timing of inhibition. If this interpretation is correct, our findings suggest that cortical neurons are more sensitive to coincident synaptic inputs than would be predicted solely on the basis of postsynaptic temporal summation.

Our observations also demonstrate that the magnitude and rate of rapid V_m depolarizations during the response to a sensory stimulus are suppressed when the cell is hyperpolarized below firing threshold. This effect may result from three possible mechanisms. First, hyperpolarization will alter the driving force acting on inhibitory synaptic currents and thereby change the amplitude or polarity of IPSPs. Second, it may also increase the membrane conductance because of anomalous rectification. This effect would be expected to reduce the amplitude of EPSPs and increase their rate of rise. While our results are consistent with the former prediction, they are inconsistent with the latter. We found that the rate of rise of the CTA was greater during control conditions. Finally, hyperpolarization will also reduce inward currents that are activated by depolarization (43). Although our findings cannot accurately discriminate among these possible mechanisms, *in vitro* studies provide some support for the latter. Excitatory synaptic inputs can be amplified by voltage-gated Na^+ (44–48) and Ca^{2+} (49–51) currents as well as NMDA synaptic currents (52). Thus, a number of voltage-gated inward currents may contribute to the amplification of excitatory synaptic input and thereby influence the amplitude and time course of V_m fluctuations leading to modification of action potential threshold.

Given what is known about spike-generating mechanisms, our finding of a dynamic threshold in cortical neurons is not unexpected, but its implications may have been underestimated. Dynamic variations in spike threshold have been observed in a number of preparations (23–27, 53) and the time course and voltage dependence of these variations are consistent with the properties of voltage-gated sodium and potassium channels (28–32). In all neurons, sodium channel activation occurs at a faster rate than inactivation. This difference in gating kinetics enables the rapid upstroke of the action potential and makes the spike-generating mechanism sensitive to the rate of V_m depolarization (28–30). Consequently, when V_m depolarizes slowly, activation and inactivation can proceed in parallel. This reduces the number of available sodium channels and increases the threshold for generating a spike. Conversely, when V_m depolarizes rapidly, there is a brief window in time in which many sodium channels will be activated but not yet inactivated. If under these conditions V_m is sufficiently depolarized, a spike can be generated at a lower threshold. Our finding that spike threshold was inversely correlated with the rising slope of the action potential is consistent with this interpretation. Thus, the basic mechanism responsible for spike generation also endows cortical neurons with enhanced sensitivity to rapid V_m depolarizations.

Methodological Considerations. The conclusions of this study rest on two major assumptions regarding the measurement of spike threshold. The first concerns the definition of threshold. One common measure, often referred to as the current threshold, is the minimum amount of current necessary to initiate a regenerative depolarization from a given resting V_m. Although this provides one accurate means for measuring threshold, it is a measure that can be obtained only under steady-state conditions and will vary with the resting V_m (54). We have chosen to define threshold as the membrane voltage at the inflection point preceding the upstroke of a spike. Although this may be an inappropriate measure of spike threshold, it was the only practical means available under the conditions of our study. The principal reason for this is that neurons *in vivo* do not exist in a steady-state condition; the membrane potential and conductance are continuously changing. Nonetheless, we believe that our measure of spike threshold accurately reflects the spike initiation process because it is well correlated with the mean V_m, mean firing rate, and instantaneous firing rate (data not shown), as well as the rate of the action potential upstroke. Each of these relationships is well predicted by the voltage dependence of the conductances underlying the action potential.

Our conclusions also rest on the assumption that our measurements of spike threshold reflect the voltage fluctuations occurring at the site of spike initiation. We generally assume, but cannot confirm, that the majority of our impalements occur at or near the soma, and we attempted to exclude putative intradendritic recordings from our sample. Several studies have reported that somatic action potentials in cortical neurons are initiated in the axon initial segment or the first node of Ranvier (55–57). Thus, our measurements of spike threshold could deviate from the actual threshold at the site of initiation if these compartments are not isopotential. Under these conditions, fluctuations of somatic V_m could obscure the threshold behavior at the site of initiation. We cannot exclude the possibility that this effect contributed to our results. However, Gogan *et al.* (55) have shown that the electronic length of the axon initial segment of spinal motoneurons is relatively short. If this is also true for cortical neurons, as suggested by Colbert and Johnston (56), the

voltage fluctuations in the first node of Ranvier and the soma should be similar. Our findings that spike threshold is correlated with the rate of change of V_m preceding a spike and the rate of the action potential upstroke are consistent with this interpretation.

Related Work. Prior studies on the relation between spike threshold and V_m time course have been largely restricted to the *in vitro* preparation (23–24, 26–27, 53). However, *in vitro* studies have obvious limitations for investigating physiological function. To our knowledge, only one report has demonstrated a relation between cellular excitability and the rate of V_m depolarization *in vivo*. This work has shown that the efficacy of an electrically evoked EPSP in triggering a spike is proportional to its rate of rise as well as its amplitude (58). This process may contribute to the shortening of the interspike interval and consequently increase the firing rate (59), but the relationship between spike threshold and the rate of V_m depolarization has not been demonstrated. In fact, the study of Fetz and Gustafsson (58) provides an alternative model that explicitly treats the spike threshold as being fixed. Here, we show that the voltage threshold of cortical neurons *in vivo* is not a fixed quantity, particularly when the cells respond to a sensory stimulus.

Functional Implications. Our findings indicate that the spike-generating mechanism may contribute to the generation of synchronous cortical activity by amplifying coincident events. Support for this comes from a recent study demonstrating that coincident dendritic inputs are amplified by voltage-gated sodium currents (48). This mechanism increases the firing probability of cortical neurons in response to synchronous inputs and thereby enhances the correlation between cellular input and output. The resulting entrained spike activity could be further propagated via local and long-range connections and could thereby act to recruit large populations of neurons into synchronously firing ensembles. In a similar manner, the dynamic threshold mechanism might enable cortical neurons to respond to time-varying stimuli with high temporal fidelity (19, 21, 60). Recently, it has been shown that neurons in extrastriate visual cortex can respond to time-varying stimuli, such as rapid coherent movements, with a temporal precision in the millisecond range (20, 22). This effect is likely to be mediated by a population of neurons at each stage in the pathway whose spike discharges are time locked to the temporal fluctuations in the stimulus. Our findings suggest that this type of stimulus-locked synchrony might propagate faithfully through neocortical structures because of the lower spike threshold that occurs in response to synchronous inputs.

We thank David McCormick for help in collecting a portion of the experimental data. We also thank Lee Rognlie-Howes for her excellent care of the animals and Dan Johnston and Shih-Cheng Yen for their valuable comments on an earlier version of the manuscript. This work was supported by grants to R.A. from the Human Frontiers Science Program and to C.M.G. from the National Eye Institute.

1. Gerstein, G. L. & Mandelbrot, B. (1964) *Biophys. J.* **4,** 41–68.
2. Stein, R. B. (1965) *Biophys. J.* **5,** 173–194.
3. Stein, R. B. (1679) *Biophys. J.* **7,** 797–826.
4. Hoopen, M. T. (1966) *Biophys. J.* **6,** 435–451.
5. Calvin, W. H. & Stevens, C. F. (1967) *J. Neurophysiol.* **31,** 574–587.
6. Nelken, I. (1988) *Biol. Cybern.* **59,** 201–215.
7. Tuckwell, H. C. (1989) *Stochastic Processes in the Neurosciences* (Soc. Indust. Appl. Math., Philadelphia, PA).
8. Shadlen, M. N. & Newsome, W. T. (1998) *J. Neurosci.* **18,** 3870–3896.
9. Carandini, M. & Ferster, D. (2000) *J. Neurosci.* **20,** 470–484.
10. Shadlen, M. N. & Newsome, W. T. (1994) *Curr. Opin. Neurobiol.* **4,** 569–579.
11. Diesmann, M., Gewaltig, M. O. & Aertsen, A. M. (1999) *Nature (London)* **402,** 529–533.
12. Abeles, M. (1982) *Isr. J. Med. Sci.* **18,** 83–92.
13. von der Malsburg, C. & Schneider, W. (1986) *Biol. Cybern.* **54,** 29–40.
14. Softky, W. R. & Koch, C. (1993) *J. Neurosci.* **13,** 334–350.
15. Konig, P., Engel, A. K. & Singer, W. (1996) *Trends Neurosci.* **19,** 130–137.
16. Abeles, M., Prut, Y., Bergman, H. & Vaadia, E. (1994) *Prog. Brain Res.* **102,** 395–404.
17. Singer, W. & Gray, C. M. (1995) *Annu. Rev. Neurosci.* **18,** 555–586.
18. Usrey, W. M. & Reid, R. C. (1999) *Annu. Rev. Physiol.* **61,** 435–456.
19. Mainen, Z. F. & Sejnowski, T. J. (1995) *Science* **268,** 1503–1506.
20. Bair, W. & Koch, C. (1996) *Neural Comput.* **8,** 1185–1202.
21. Nowak, L. G., Sanchez-Vives, M. V. & McCormick, D. A. (1997a) *Cereb. Cortex* **7,** 487–501.
22. Buracas, G. T., Zador, A. M., DeWeese, M. R. & Albright, T. D. (1998) *Neuron* **20,** 959–969.
23. Vallbo, A. B. (1964) *Acta Physiol. Scand.* **61,** 429–444.
24. Frankenhaeuser, B. & Vallbo, A. B. (1965) *Acta Physiol. Scand.* **63,** 1–20.
25. Calvin, W. H. (1974) *Brain Res.* **69,** 341–346.
26. Schlue, W. R., Richter, D. W., Mauritz, K. H. & Nacimiento, A. C. (1973) *J. Neurophysiol.* **37,** 303–309.
27. Stafstrom, C. E., Schwindt, P. C., Flatman, J. A. & Crill, W. E. (1984) *J. Neurophysipol.* **52,** 244–263.
28. Hodgkin, A. L. & Huxley, A. F. (1952a) *J. Physiol. (London)* **116,** 497–506.
29. Hodgkin, A. L. & Huxley, A. F. (1952b) *J. Physiol. (London)* **117,** 500–544.
30. Noble, D. & Stein, R. B. (1966) *J. Physiol. (London)* **187,** 129–161.
31. Noble, D. (1966) *Physiol. Rev.* **46,** 1–50.
32. Armstrong, C. M. (1992) *Physiol. Rev.* **72,** S5–S13.
33. Azouz, R. & Gray, C. M. (1999) *J. Neurosci.* **19,** 2209–2223.
34. Gray, C. M. & McCormick, D. A. (1996) *Science* **274,** 109–113.
35. Azouz, R., Gray, C. M., Nowak, L. G. & McCormick, D. A. (1997) *Cereb. Cortex* **7,** 534–545.
36. Connors, B. W., Gutnick, M. J. & Prince, D. A. (1982) *J. Neurophysiol.* **48,** 1302–1320.
37. McCormick, D. A., Connors, B. W., Lighthall, J. W. & Prince, D. A. (1985) *J. Neurophysiol.* **54,** 782–806.
38. Hines, M. (1989) *Int. J. Biomed. Comput.* **24,** 55–68.
39. Huguenard, J. R., Hamill, O. P. & Prince, D. A. (1988) *J. Neurophysiol.* **59,** 778–795.
40. Belluzzi, O. & Sacchi, O. (1991) *Prog. Biophys. Mol. Biol.* **55,** 1–30.
41. Colbert, C. M., Magee, J. C., Hoffman, D. A. & Johnston, D. (1997) *J. Neurosci.* **17,** 6512–6521.
42. Carandini, M., Mechler, F., Leonard, C. S. & Movshon, J. A. (1996) *J. Neurophysiol.* **76,** 3425–3441.
43. Haag, J. & Borst, A. (1996) *Nature (London)* **379,** 639–641.
44. Hirsch, J. A. & Gilbert, C. D. (1991) *J. Neurosci.* **11,** 1800–1809.
45. Schwindt, P. C. & Crill, W. E. (1995) *J. Neurophysiol.* **74,** 2220–2224.
46. Stuart, G. & Sakmann, B. (1995) *Neuron* **15,** 1065–1076.
47. Lipowsky, R., Gillessen, T. & Alzheimer, C. (1996) *J. Neurophysiol.* **76,** 2181–2191.
48. Margulis, M. & Tang, C. M. (1998) *J. Neurophysiol.* **79,** 2809–2813.
49. Deisz, R. A., Fortin, G. & Zieglgänsberger, W. (1991) *J. Neurophysiol.* **65,** 371–382.
50. Gillessen, T. & Alzheimer, C. (1997) *J. Neurophysiol.* **77,** 1639–1643.
51. Schiller, J., Schiller, Y., Stuart, G. & Sakmann, B. (1997) *J. Physiol. (London)* **505,** 605–616.
52. Thomson, A. M., Girdlestone, D. & West, D. C. (1988) *J. Neurophysiol.* **60,** 1896–1907.
53. Heck, D., Rotter, S. & Aertsen, A. (1993) in *Brain Theory*, ed. Aertsen, A. (Elsevier, Amsterdam), pp. 241–249.
54. Jack, J. J. B., Noble, D. & Tsien, R. W. (1983) *Electric Current Flow in Excitable Cells* (Clarendon, Oxford).
55. Gogan, P., Gueritaud, J. P. & Tyc-Dumont, S. (1983) *J. Physiol. (London)* **335,** 205–220.
56. Colbert, C. M. & Johnston, D. (1996) *J. Neurosci.* **16,** 6676–6686.
57. Stuart, G., Schiller, J. & Sakmann, B. (1997) *J. Physiol. (London)* **505,** 617–632.
58. Fetz, E. E. & Gustafsson, B. (1983) *J. Physiol. (London)* **341,** 387–410.
59. Reyes, A. D. & Fetz, E. E. (1993) *J. Neurophysiol.* **69,** 1661–1672.
60. Aertsen, A. M., Smolders, J. W. & Johannesma, P. I. (1979) *Biol. Cybern.* **32,** 175–185.